Original Research

Detailed Analysis of Myocardial Motion in Volunteers and Patients Using High-Temporal-Resolution MR Tissue Phase Mapping

Bernd Jung, PhD,[1]* Daniela Föll, MD,[2] Petra Böttler, MD,[3] Steffen Petersen, MD,[4] Jürgen Hennig, PhD,[1] and Michael Markl, PhD[1]

Purpose: To detect and investigate details in left ventricular (LV) motion patterns with a temporal resolution comparable to that of echocardiography.

Material and Methods: To assess global and regional myocardial motion in high temporal detail, respiratory-gated MR phase-contrast measurements with three-directional velocity encoding (venc) were performed in 12 healthy volunteers and two patients with LV hypertrophy in basal, midventricular, and apical locations of the LV with a temporal resolution of 13.8 msec.

Results: The volunteer data revealed details in LV motion patterns that were known only from echocardiography. For all volunteers, characteristic myocardial motion patterns, such as triphasic global diastolic expansion, could be detected with high accuracy. One volunteer underwent an additional echocardiographic measurement in order to corroborate the complex motion features as measured by MRI. Patient examinations revealed substantial changes in diastolic function compared to motion patterns in healthy volunteers.

Conclusion: The proposed high-temporal-resolution velocity-mapping technique provides previously undetectable information on LV performance, and is highly promising for the detection of local and global motion abnormalities in patients with disturbed LV performance, such as diastolic dysfunction.

Key Words: phase contrast; cardiac function; myocardial motion; respiratory gating; diastolic dysfunction
J. Magn. Reson. Imaging 2006;24:1033–1039.

ABNORMAL REGIONAL LEFT VENTRICULAR (LV) wall motion is an important clinical marker for multiple cardiac pathologies, and its diagnosis is of critical importance. Diastolic dysfunction accounts for up to half of all heart-failure cases (1). Many experimental studies suggest that regional myocardial relaxation disorders are related to specific cardiac diseases, such as ischemic or hypertrophic cardiomyopathy and LV hypertrophy (2–6).

Tissue Doppler imaging (TDI) is a well-established method that allows the noninvasive assessment of regional LV function (7), which can be used to perform a detailed analysis of diastolic function (8,9). The drawbacks of TDI are related to limitations of the acoustic window due to interferences from bone or lung. In addition, pulsed Doppler techniques such as TDI can result in low velocity resolution and unreliable measurements (7). Furthermore, TDI lacks spatial information and myocardial velocities are affected by the angle of insonation of the ultrasound beam from the transducer (10). The benefit of TDI is that it can provide a high temporal resolution of up to 5 msec, which allows for a detailed analysis of myocardial motion and results in characteristic findings in normal subjects (e.g., a small biphasic wave) within a short temporal window of 50 msec during isovolumetric relaxation (IVR) (11,12). Due to the brief duration of such motion patterns, high temporal resolution is necessary to detect and investigate any changes in these patterns related to LV disease.

MRI provides noninvasive tools for investigating myocardial function that have the potential to overcome the limitations of TDI. In addition to techniques for assessing qualitative and quantitative global wall motion with cine imaging, such as balanced SSFP, methods for assessing regional and global heart wall motion have been introduced (13,14). Established methods for quantitative analysis of myocardial wall motion include tagging (15), phase-contrast velocity mapping (tissue phase mapping (TPM)) (16), and displacement encoding with stimulated echoes (DENSE) (17). These methods can be used to extract parameters such as strain or radial and tangential (circumferential) velocity components (18,19). TPM and DENSE offer high spatial resolution of the functional information (1–3 mm), which is limited in tagging by the number and density of the tag lines (4–8 mm). In contrast to the recently presented two-dimen-

[1]Department of Diagnostic Radiology, Medical Physics, University Hospital, Freiburg, Germany.
[2]Department of Cardiology, University Hospital, Freiburg, Germany.
[3]Department of Pediatric Cardiology, University Hospital, Freiburg, Germany.
[4]Department of Cardiovascular Medicine, John Radcliffe Hospital, Oxford, United Kingdom.
*Address reprint requests to: B.J., Department of Diagnostic Radiology, Medical Physics, Freiburg University, Hugstetterstr. 55, 79106 Freiburg, Germany. E-mail: bernd.jung@uniklinik-freiburg.de
Received November 3, 2005; Accepted June 30, 2006.
DOI 10.1002/jmri.20703
Published online 31 August 2006 in Wiley InterScience (www.interscience.wiley.com).

sional (2D)-Cine-DENSE method (20), TPM provides time-resolved information and a constant signal-to-noise ratio (SNR) over the cardiac cycle. For breath-held TPM and Cine-DENSE, the temporal resolution is typically in the range of 60–80 msec, while tagging provides a somewhat higher temporal resolution of 20–40 msec, depending on the breath-holding capability of the investigated subject. Recently a high correlation between TPM and TDI measurements for the analysis of LV myocardial velocities was demonstrated in healthy volunteers (21).

Since data acquisition with TPM is typically based on multiple breath-held 2D measurements (22,23), the spatial and temporal resolution are limited due to the length of the breath-hold period. A potential solution to this drawback may be found in a recently reported method for high-temporal-resolution velocity mapping using multiple breath-hold scans for reference and sensitive scans (24). However, separate breath-holds may result in a slight variability in heart position between different scans. To overcome these limitations related to breath-holding, we used a prospective respiratory gating technique with two navigators and paired acceptance criteria for the acquisition of TPM data (25). This gating technique allows a robust suppression of respiration artifacts and corruption of the measured tissue velocities while maintaining high scan efficiency. As a result, limitations with respect to the total scan duration are effectively removed and permit the acquisition of TPM images with flexible and high temporal and spatial resolution. Phase-contrast measurements with three-directional velocity encoding (venc) were performed in a study with 12 healthy volunteers with a temporal resolution of 13.8 msec. One volunteer underwent an additional TDI examination in order to verify the complex motion pattern as measured by TPM. Furthermore, TPM data were acquired in two patients with LV hypertrophy with the same temporal resolution as in the volunteer examinations.

MATERIALS AND METHODS

Data Acquisition

All measurements were performed on a 1.5 T Magnetom Sonata (Siemens Medical Solutions, Erlangen, Germany). TPM images were acquired in 12 volunteers (mean age = 32 years, range = 23–65 years) and two patients with LV hypertrophy (mean age = 38 years, range = 32–43 years). The human studies were approved by the local ethics committee of our institution, and informed consent was obtained from all subjects.

A black-blood *k*-space segmented gradient-echo sequence (TR = 6.9 msec, flip angle = 15°, bandwidth = 650 Hz/pixel) with first-order flow compensation was used for data acquisition. The pixel size was 1.3 × 1.3 mm (96 × 256 matrix interpolated to 192 × 256). We performed venc by adding a bipolar gradient with a venc of 15 cm/s in-plane and 25 cm/s through-plane according to typical velocity values observed in the wall motion of the LV.

Advanced navigator respiratory gating was performed using two navigator echoes per cardiac cycle in combination with real-time acceptance criteria based on signal from successive navigator echo pairs, in the middle and at the end of the cardiac cycle, as recently described (25). The total time required for the navigators and their evaluation was 40 msec. Data were accepted when the current diaphragm position was inside a 6-mm acceptance window in end-expiration.

To achieve high temporal resolution, reference and motion-sensitized scans were performed in a sequential manner (i.e., in consecutive cardiac cycles), since an interleaved venc order limits the minimal temporal resolution to 4 * TR = 27.6 msec for a given TR. In addition, view-sharing (as described previously (26)) was implemented for sequential venc, resulting in a temporal resolution of 13.8 msec. Full three-directional velocity information from the beating heart for 96 phase encodings was obtained in 128 heartbeats, assuming a scan efficiency of 100%. Three slices with a slice thickness of 8 mm were acquired in the short-axis plane, in basal, midventricular, and apical locations.

To compare the velocity time courses obtained by MRI, we performed TDI measurements in one healthy subject with a current standard ultrasound machine (General Electric, Vivid 7). Data from regional myocardial velocity profiles of the longitudinal component (shortening/lengthening of the long axis) were acquired in a midventricular anteroseptal region with a temporal resolution of 9.5 msec and compared with a corresponding regional analysis of the TPM data for the same volunteer.

Postprocessing

Data postprocessing was performed on a personal computer using customized software programmed in Matlab (The Mathworks Inc., Natick, MA, USA). Following contour segmentation (manual contour definition using snakes) and bulk motion correction based on subtraction of global translation velocities from the local velocity components (19), the measured in-plane velocities were transformed into an internal polar coordinate system positioned at the center of mass of the segmented LV. As a result, the motional parameters are described in terms of a cylindrical coordinate system based on radial (contraction/expansion), circumferential (rotation, twisting), and longitudinal (shortening/lengthening) velocities, leading to a more adapted representation of myocardial motion.

To investigate regional variations in myocardial velocities, we visualized the vector field plots and color-coded maps for each velocity component for each phase of the cardiac cycle. For better orientation, velocity vector fields and motion components were overlaid onto corresponding anatomical images (see also Fig. 2) . For the analysis of global cardiac motion features, velocity components were averaged over the entire segmentation mask, resulting in velocity time courses in basal, midventricular, and apical locations for each volunteer. For a cumulative assessment of myocardial motion, the obtained time courses were averaged over all volunteers for each acquired slice and each velocity component. To avoid temporal jitter, time series were normalized to the end-systolic time, as defined by the first minimum peak

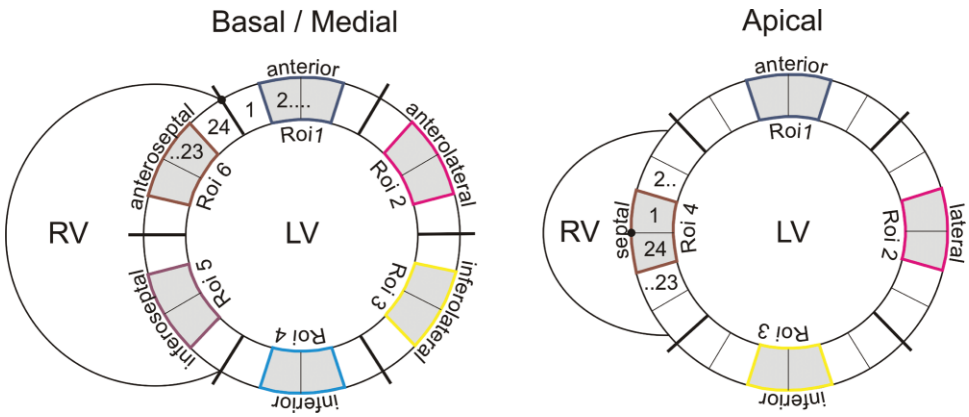

Figure 1. ROI analysis in 16 segments according to AHA/ACC recommendations. Each acquired slice of the LV was subdivided into 24 segments. Mean velocities were calculated inside every segment according to the 16-segment model.

of the global radial velocities during diastole (see Fig. 3), which could be observed in all volunteer measurements. Since the length of the diastolic period indicated by the time point after expansion with zero velocities was the same for all volunteer measurements, the diastolic period was not normalized separately.

To analyze local differences in LV performance, we performed an ROI analysis based on the 17-segment model according to American Heart Association (AHA) and American College of Cardiology (ACC) recommendations (27). Each acquired slice of the LV was subdivided into 24 angular segments. The mean velocities were calculated as illustrated in Fig. 1 to generate regional velocity time courses in six basal, six midventricular, and four apical regions according to the 17-segment model (the 17th purely apical segment was excluded from this analysis).

For comparison of TDI and TPM measurements, an ROI was chosen in the midventricular anteroseptal region in the TPM images, and the mean longitudinal velocities within the region were calculated from the TPM data. Both TPM and TDI velocity time courses were drawn in a single graph and temporally normalized to the upslope of velocities during early systole. To visually aid the comparison of both data sets, the time course measured by TPM was interpolated to the slightly higher temporal resolution (9.5 msec) of the TDI data.

RESULTS

The mean scan efficiency over all acquired slices was 43%, resulting in an acquisition duration of about 4.5 minutes per slice. The total scan time for a volunteer measurement was about 20 minutes, including positioning and planning of the short-axis TPM scans.

Figure 2 shows magnitude images (upper row) in a basal slice of a data set with a temporal resolution of 13.8 msec acquired during free breathing. Five characteristic cardiac frames are shown: early systole (during isovolumetric contraction (IVC); Fig. 2a), mid-systole (Fig. 2b), early diastole (during IVR; Fig. 2c), mid-diastole (Fig. 2d), and late diastole (Fig. 2e). Corresponding color-coded maps of radial velocities are shown in the middle row, and pixelwise arrow plots of in-plane velocity vector fields are shown in the lower row. During early systole, in-plane motion is mainly determined by a counterclockwise rotation, whereas in mid-systole the rotational direction has changed and myocardial motion includes high radial components (red: positive velocities) that describe the contraction of the LV. The

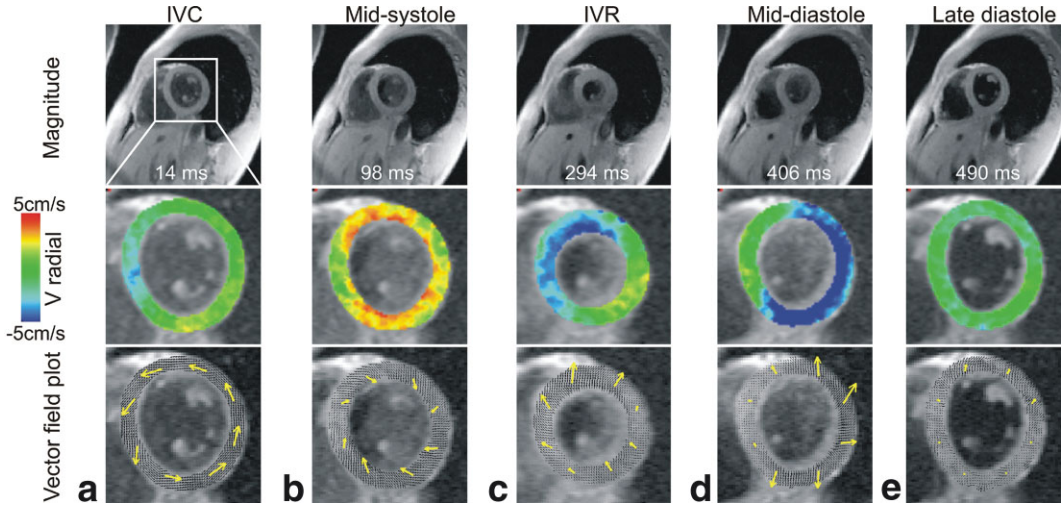

Figure 2. Magnitude images (upper row), color-coded maps of radial velocities (middle row), and pixelwise arrow plots of in-plane velocity vector fields (lower row) in a basal slice for five cardiac frames (isovolumetric contraction/relaxation (IVC/IVR). The data set of a healthy volunteer was acquired during free breathing with a temporal resolution of 13.8 msec.

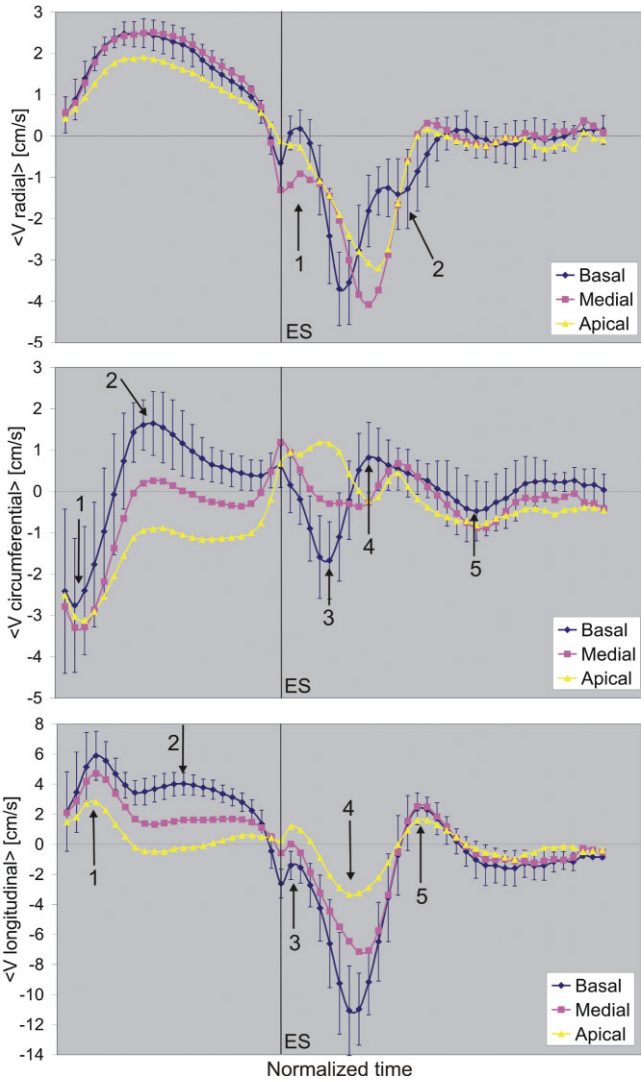

Figure 3. Time courses of radial (top), circumferential (middle), and longitudinal (bottom) velocities with high temporal resolution averaged over all volunteers. Each graph shows a comparison of data for basal, midventricular, and apical slice locations. ES = end-systole. [Color figure can be viewed in the online issue, which is available at www.interscience.wiley.com.]

highest radial velocities occur in the endocardial region, which is mainly responsible for myocardial wall thickening. During early diastole regional anteroseptal expansion (indicated by negative radial velocities (blue)) precedes other LV areas and the inferolateral region shows a slight contraction (see also Fig. 4). During mid-diastole the main part of the myocardial wall expands (except for the septum, which expands somewhat later; results not shown). No significant motion components were detected in late diastole.

Figure 3 shows the averaged time courses over all volunteers for radial (contraction/expansion, top), circumferential (rotation, middle), and longitudinal (lengthening/shortening, bottom) velocities with high temporal resolution. For each motion component, global velocity time courses are plotted for basal, midventricular, and apical slices to allow for direct comparison of LV performance in different locations. Note the low interindividual variability as indicated by the small standard deviations (SDs; shown only for the basal slice for better visualization).

Radial velocities (Fig. 3, top) evolved similarly during systole in all locations, whereas motion patterns during diastole were successfully resolved in high temporal detail and demonstrated a somewhat different behavior. A small biphasic pattern during early diastole is clearly visible in all slices (arrow 1). The diastolic peak velocity occurs later in locations toward the apex. Furthermore, the basal slice shows the above-mentioned triphasic diastolic expansion, as indicated by a third negative peak in the later diastole (arrow 2).

The circumferential velocities (Fig. 3, middle) demonstrate considerable differences between the apical and basal slices, indicating that the well-known velocity twist (counter-rotation of basal vs. apical slices) occurred during mid-systole. During diastole the circumferential velocities show a different and complex motion pattern in different slice locations. For example, basal slices undergo five identifiable changes of rotational direction during a single cardiac cycle (arrows 1–5), indicating a highly complex rotational behavior of normal myocardial motion.

The motion pattern of the longitudinal velocities (Fig. 3, bottom) is similar in all slices except for decreasing amplitudes toward the apex. Systolic motion shows an initial displacement toward the apex (arrow 1) followed by a velocity decrease, and ending in a distinct increase of velocities near end-systole (arrow 2). The small biphasic pattern during early diastole for all slice locations, which was also observed for radial velocities during the same cardiac phase, is clearly visible (arrow 3). Following rapid motion toward the base during diastole (arrow 4), the longitudinal motion patterns demonstrate an overshoot (increased longitudinal lengthening before returning to the equilibrium position prior to the next systolic contraction) in all three slices, as indicated by the positive velocity peaks (arrow 5).

Figure 4 shows the evolution of regional radial velocities averaged over all volunteers in the ROIs depicted in Fig. 1 (the SDs were again omitted for better visualization). The systolic velocity time courses are similar in all segments (except for the amplitudes), whereas motion patterns during diastole exhibit considerably different local ventricular expansion in segments inside a single slice and between different slices.

Notably, the septum demonstrates highly complex motion patterns (brown and violet lines), especially in the basal slice, where much lower peak velocities occur, indicating distinct differences in regional expansion behavior. The early diastolic biphasic pattern (arrow 1 in Fig. 4, top and middle) can be observed in all ROIs and is most evident in basal and midventricular locations, but with different amplitudes. An overshoot after the rapid relaxation during diastole similar to the longitudinal velocities (see Fig. 3) can be observed in the anterior and inferolateral regions of the midventricular slice (middle, arrow 2).

Figure 5 shows a comparison of regional longitudinal time courses between TDI (yellow) and TPM (blue) ac-

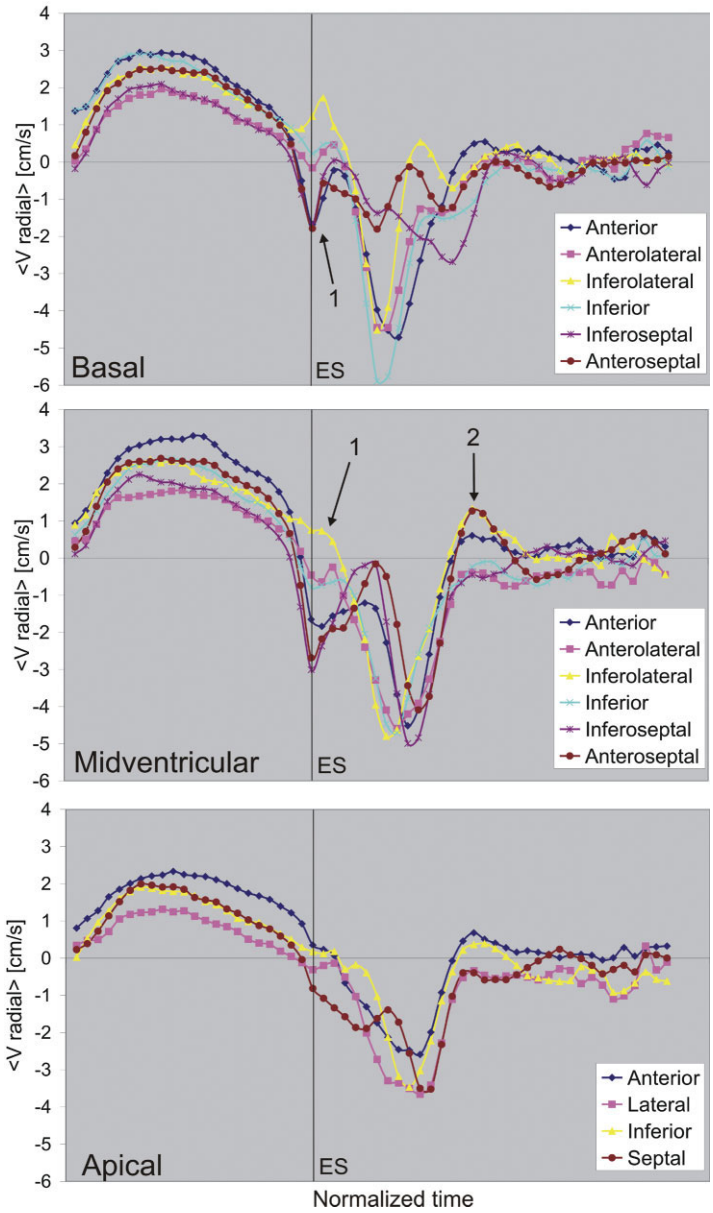

Figure 4. Regional time courses of radial velocities with high temporal resolution according to the 16-segment model in the three acquired slices averaged over all volunteers. ES = end-systole.

quired in a healthy volunteer. Complex motion patterns, such as the small biphasic wave of brief duration during IVR in early diastole, are clearly visible in both measurements, indicating that ventricular dynamics that were previously not seen with MRI can be detected and correlated with TDI data with the use of high-temporal-resolution TPM.

Figure 6 shows an example of a patient with LV hypertrophy. The time courses of the patient (blue) and time courses averaged over all healthy volunteers (yellow) are drawn on the same graph (global radial velocities in a midventricular slice location (top), and global longitudinal velocities in a basal slice location (bottom)). It is evident that the motion patterns during diastole are prolonged and the peak velocities are reduced. The small biphasic pattern during early diastole (see also Fig. 4, arrow 3) is strongly reduced for the time course of longitudinal velocities (b).

DISCUSSION

We have presented an efficient strategy for combining TPM acquisition and navigator respiratory gating that permits the acquisition of TPM data with high temporal resolution. The dual navigator gating technique combined with paired acceptance/rejection criteria allows for a robust suppression of respiration artifacts, as illustrated by the magnitude images in Fig. 1. All measurements revealed detailed motion patterns (e.g., the short but distinct biphasic expansion pattern during IVR) during a large fraction of the cardiac cycle, and especially during diastole, that were previously known only from diffusion tensor imaging (DTI) measurements (11,12).

The high-temporal-resolution data obtained in this study provide much more detail about global contraction and expansion patterns, such as additional peaks during diastole, compared to previously reported

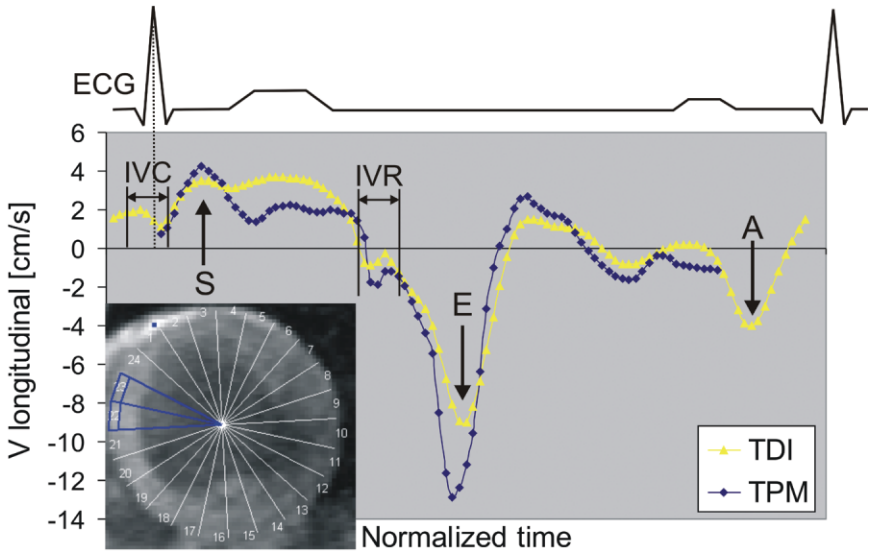

Figure 5. Comparison of regional longitudinal velocities in a midventricular anteroseptal area measured by TDI and TPM in the same healthy volunteer. [Color figure can be viewed in the online issue, which is available at www.interscience.wiley.com.]

breath-hold measurements (22). The dynamics of myocardial motion patterns revealed by high-temporal-resolution TPM measurements can also be corroborated by TDI measurements. A detailed comparison between TDI and TPM in well-defined myocardial points in a large group of healthy volunteers was recently performed with a somewhat lower temporal resolution (21). In addition, a previous study compared breath-hold measurements with a lower temporal resolution and free-breathing measurements with a high temporal resolution (25).

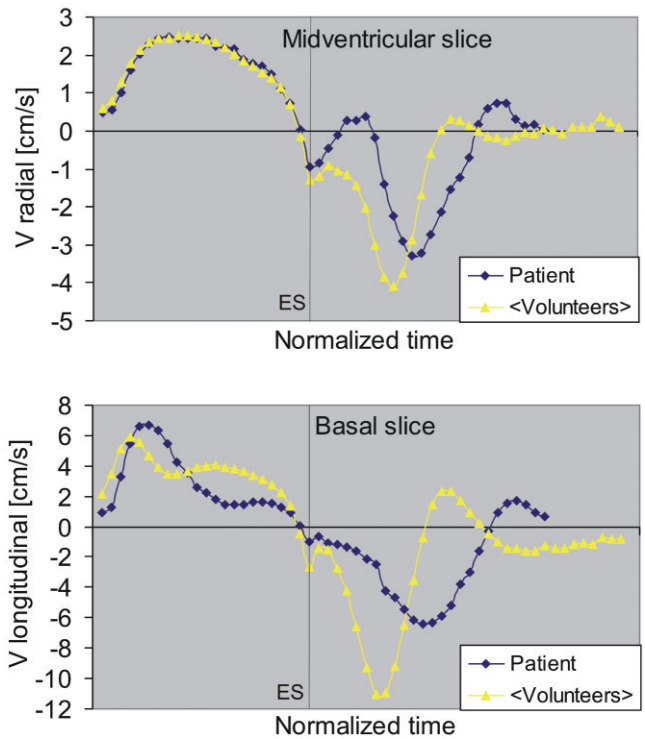

Figure 6. Global time courses of radial velocities in a midventricular slice (top) and longitudinal velocities in a basal slice (bottom) in a patient with LV hypertrophy, and averaged over all volunteers. ES = end-systole. [Color figure can be viewed in the online issue, which is available at www.interscience.wiley.com.]

The presented comparison of TDI and TPM measurements focused on the verification of the complex motion patterns, and not on a quantitative comparison of peak velocities. While the shape of local longitudinal motion patterns exhibited excellent agreement, velocity amplitudes were somewhat different from each other. This disagreement may be explained by the dependence of the amplitudes in TDI measurements on the angle of insonation of the ultrasound beam from the transducer. Further volunteer and patient studies and more extensive comparisons between both modalities are needed to validate and explore the limitations of each technique.

Because we used prospective gating in this study, the A-wave (see Fig. 3) in late diastole caused by the contraction of the left atrium and the IVC phase (Fig. 5) cannot be seen by the TPM measurements. The use of a retrospective gating technique could provide these motion features during late diastole. Future improvements therefore include the implementation of retrospective gating to allow full coverage of the cardiac cycle (with the exception of the time needed for navigator execution and evaluation). However, since many specific cardiac diseases are related to regional myocardial relaxation disorders, the current TPM measurements provide the most important information during the cardiac cycle.

The results of the patient examinations showed clear differences in motion patterns compared to the healthy volunteers. Specifically, patients with LV hypertrophy demonstrated a prolongation of diastolic motion patterns and a clear reduction of peak velocities.

The presented TPM measurements suggest that the high-temporal-resolution technique may be valuable for assessing the efficacy of pharmaceutical or other therapeutic procedures. Specific cardiac diseases known from TDI measurements that may be suitable for TPM investigations include ischemic cardiomyopathy (2), hypertrophic cardiomyopathy (3), heart trans-

plant recipients (4), LV hypertrophy (5), and differentiating constrictive pericarditis from restrictive cardiomyopathy (6). It has been suggested that regional relaxation dysfunction induces a prolongation of the IVR in ischemic cardiomyopathy (2).

It should be noted, however, that the data presented here were acquired in young, healthy volunteers. A clinically valid reference standard would require a larger database and especially data from different age groups to permit a correlation of local motion patterns between age-matched volunteers and patients with potentially disturbed myocardial motion. Further studies at our institution are already under way to examine age-related differences in cardiac motion and to generate a database for future clinical applications.

A technical limitation of this study is the long acquisition time needed to acquire TPM data for a single slice. The scan time may be reduced by the use of radial acquisition strategies with interleaved undersampled projections for 2D and 3D phase-contrast data (28). Additional scan time reduction could be achieved by using parallel imaging techniques, such as sensitivity encoding (SENSE) and generalized autocalibrating partially parallel acquisitions (GRAPPA) (29,30), in combination with imaging at the higher field strength to compensate for the SNR loss associated with parallel imaging (31).

In conclusion, high-temporal-resolution TPM provides insights into global and local myocardial wall motion with high spatial and temporal detail. The resulting myocardial velocities obtained in volunteers and patients show that this method has the potential to provide valuable information for evaluating global and regional systolic and diastolic function in cardiac pathologies.

REFERENCES

1. Vasan RS, Levy D. Defining diastolic heart failure: a call for standardized diagnostic criteria. Circulation 2000;101:2118–2121.
2. Garcia-Fernandez MA, Azevedo J, Moreno M, et al. Regional diastolic function in ischaemic heart disease using pulsed wave Doppler tissue imaging. Eur Heart J 1999;20:496–505.
3. Nagueh SF, Bachinski LL, Meyer D, et al. Tissue Doppler imaging consistently detects myocardial abnormalities in patients with hypertrophic cardiomyopathy and provides a novel means for an early diagnosis before and independently of hypertrophy. Circulation 2001;104:128–130.
4. Puleo JA, Aranda JM, Weston MW, et al. Noninvasive detection of allograft rejection in heart transplant recipients by use of Doppler tissue imaging. J Heart Lung Transplant 1998;17:176–184.
5. Rodriguez L, Garcia M, Ares M, Griffin BP, Nakatani S, Thomas JD. Assessment of mitral annular dynamics during diastole by Doppler tissue imaging: comparison with mitral Doppler inflow in subjects without heart disease and in patients with left ventricular hypertrophy. Am Heart J 1996;131:982–987.
6. Garcia MJ, Rodriguez L, Ares M, Griffin BP, Thomas JD, Klein AL. Differentiation of constrictive pericarditis from restrictive cardiomyopathy: assessment of left ventricular diastolic velocities in longitudinal axis by Doppler tissue imaging. J Am Coll Cardiol 1996; 27:108–114.
7. De Boeck BW, Cramer MJ, Oh JK, van der Aa RP, Jaarsma W. Spectral pulsed tissue Doppler imaging in diastole: a tool to increase our insight in and assessment of diastolic relaxation of the left ventricle. Am Heart J 2003;146:411–419.
8. Muscholl M, Dennig K, Kraus F, Rudolph W. [Echocardiographic and Doppler echocardiographic characterization of left ventricular diastolic function]. Herz 1990;15:377–392.
9. Garcia-Fernandez MA, Azevedo J, Moreno M, Bermejo J, Moreno R. Regional left ventricular diastolic dysfunction evaluated by pulsed-tissue Doppler echocardiography. Echocardiography 1999;16:491–500.
10. Uematsu M, Miyatake K, Tanaka N, et al. Myocardial velocity gradient as a new indicator of regional left ventricular contraction: detection by a two-dimensional tissue Doppler imaging technique. J Am Coll Cardiol 1995;26:217–223.
11. Hammermeister KE, Gibson DG, Hughes D. Regional variation in the timing and extent of left ventricular wall motion in normal subjects. Br Heart J 1986;56:226–235.
12. Garcia MJ, Rodriguez L, Ares M, et al. Myocardial wall velocity assessment by pulsed Doppler tissue imaging: characteristic findings in normal subjects. Am Heart J 1996;132:648–656.
13. McVeigh ER. MRI of myocardial function: motion tracking techniques. Magn Reson Imaging 1996;14:137–150.
14. Masood S, Yang GZ, Pennell DJ, Firmin DN. Investigating intrinsic myocardial mechanics: the role of MR tagging, velocity phase mapping, and diffusion imaging. J Magn Reson Imaging 2000;12:873–883.
15. Zerhouni EA, Parish DM, Rogers WJ, Yang A, Shapiro EP. Human heart: tagging with MR imaging—a method for noninvasive assessment of myocardial motion. Radiology 1988;169:59–63.
16. Pelc LR, Sayre J, Yun K, et al. Evaluation of myocardial motion tracking with cine-phase contrast magnetic resonance imaging. Invest Radiol 1994;29:1038–1042.
17. Aletras AH, Ding S, Balaban RS, Wen H. DENSE: displacement encoding with stimulated echoes in cardiac functional MRI. J Magn Reson 1999;137:247–252.
18. Denney TS, Jr., McVeigh ER. Model-free reconstruction of three-dimensional myocardial strain from planar tagged MR images. J Magn Reson Imaging 1997;7:799–810.
19. Hennig J, Schneider B, Peschl S, Markl M, Krause T, Laubenberger J. Analysis of myocardial motion based on velocity measurements with a black blood prepared segmented gradient-echo sequence: methodology and applications to normal volunteers and patients. J Magn Reson Imaging 1998;8:868–877.
20. Kim D, Gilson WD, Kramer CM, Epstein FH. Myocardial tissue tracking with two-dimensional cine displacement-encoded MR imaging: development and initial evaluation. Radiology 2004;230: 862–871.
21. Jung B, Schneider B, Markl M, Saurbier B, Geibel A, Hennig J. Measurement of left ventricular velocities: phase contrast MRI velocity mapping versus tissue-Doppler-ultrasound in healthy volunteers. J Cardiovasc Magn Reson 2004;6:777–783.
22. Markl M, Schneider B, Hennig J. Fast phase contrast cardiac magnetic resonance imaging: improved assessment and analysis of left ventricular wall motion. J Magn Reson Imaging 2002;15:642–653.
23. Petersen SE, Jung BA, Wiesmann F, et al. Myocardial tissue phase mapping with cine phase-contrast mr imaging: regional wall motion analysis in healthy volunteers. Radiology 2006;238:816–826.
24. Thompson RB, McVeigh ER. High temporal resolution phase contrast MRI with multiecho acquisitions. Magn Reson Med 2002;47: 499–512.
25. Jung B, Zaitsev M, Hennig J, Markl M. Navigator gated high temporal resolution tissue phase mapping of myocardial motion. Magn Reson Med 2006;55:937–942.
26. Markl M, Hennig J. Phase contrast MRI with improved temporal resolution by view sharing: k-space related velocity mapping properties. Magn Reson Imaging 2001;19:669–676.
27. Cerqueira MD, Weissman NJ, Dilsizian V, et al. Standardized myocardial segmentation and nomenclature for tomographic imaging of the heart: a statement for healthcare professionals from the Cardiac Imaging Committee of the Council on Clinical Cardiology of the American Heart Association. Circulation 2002;105:539–542.
28. Barger AV, Peters DC, Block WF, et al. Phase-contrast with interleaved undersampled projections. Magn Reson Med 2000;43:503–509.
29. Pruessmann KP, Weiger M, Scheidegger MB, Boesiger P. SENSE: sensitivity encoding for fast MRI. Magn Reson Med 1999;42:952–962.
30. Griswold MA, Jakob PM, Heidemann RM, et al. Generalized autocalibrating partially parallel acquisitions (GRAPPA). Magn Reson Med 2002;47:1202–1210.
31. Thunberg P, Karlsson M, Wigstrom L. Accuracy and reproducibility in phase contrast imaging using SENSE. Magn Reson Med 2003; 50:1061–1068.